PROCEEDINGS OF SCIENCE

Automated Activation Procedure for GaAs Photocathodes at Photo-CATCH[†]

Maximilian Herbert,[a,*] **Tobias Eggert,**[a] **Joachim Enders,**[a] **Markus Engart,**[a] **Yuliya Fritzsche**[a] **and Vincent Wende**[a]

[a] *Institut für Kernphysik, Fachbereich Physik, Technische Universität Darmstadt, Schlossgartenstr. 9, 64289 Darmstadt, Germany*

E-mail: mherbert@ikp.tu-darmstadt.de

Photo-electron sources using GaAs-based photocathodes are used to provide high-brightness and high-current beams of (spin-polarized) electrons for accelerator applications such as free-electron lasers (FELs) and energy recovery linacs (ERLs). Such cathodes require a thin surface layer to achieve negative electron affinity (NEA) for photoemission. The layer is deposited during an activation procedure that greatly influences the resulting quantum efficiency of the photocathode and robustness of the layer. To standardize this process, the automatization of the activation procedure is investigated for operational use in an accelerator.

This contribution presents first proof-of-principle studies of a basic automated activation procedure at TU Darmstadt's EPICS-controlled photocathode test stand Photo-CATCH. Using a co-deposition scheme with Cs and O_2, several automated activations have been performed. Eight out of nine consecutive automated activations were successful, yielding a mean quantum efficiency of (4.9 ± 0.8) %, corresponding to a factor of 0.8 ± 0.2 relative to manual operation, and reproducibility to within ± 15 %.

19th Workshop on Polarized Sources, Targets and Polarimetry (PSTP2022),
26-30 September, 2022
Mainz, Germany

[†]Work supported by DFG (GRK 2128 "AccelencE", project number 264883531) and BMBF (05H18RDRB1)
[*]Speaker

PoS(PSTP2022)003

1. Introduction

High-current electron beams with a high degree of spin-polarization are in demand for a multitude of state-of-the-art particle accelerator applications such as energy-recovery linacs (ERLs [1, 2]), positron sources [3, 4] and colliders [5–7]. Direct-current (DC) high-voltage (HV) photo-emission guns using negative electron affinity (NEA) gallium arsenide (GaAs) photocathodes are currently the best available source to provide these required beam parameters.
The most important parameters of a GaAs photocathode are its quantum efficiency η and its lifetime τ. The former is proportional to the ratio of emitted photocurrent to incident laser photons, characterizing the effectiveness of photoemission from the cathode depending on the wavelength. The latter is defined as the time it takes for η to drop to $1/e$ of its original value, assuming a single-exponential decay behavior of $\eta(t)$. This decline of η over time is caused by deterioration of the NEA surface layer that is required for effective electron emission with high degree of spin-polarization. Deteriorating factors are environmental and operational effects in the electron gun, such as residual gas adsorption and ion back-bombardment (IBB). Both η and τ depend heavily on the quality of the surface layer. Therefore, the process of applying the layer to the photoacthode surface, commonly referred to as activation process, is of great importance. It largely relies on real-time operator input to achieve optimal values for both η and τ. For operational use in an accelerator, it is of great interest to simplify the process in order to make it independent from expert input. Hence, an automatization of the activation procedure would be of great benefit to accelerator operation of GaAs electron sources.
The Institute for Nuclear Physics (IKP) at the Technische Universität Darmstadt (TUDa) operates the ERL-capable Superconducting Darmstadt Linear electron Accelerator (S-DALINAC [8, 9]). Its Spin-Polarized Injector (SPIn) features a DC electron gun operating with GaAs photocathodes [10]. Additionally, a separate dedicated test stand for Photo-Cathode Activation, Testing, and Cleaning using atomic Hydrogen (Photo-CATCH) is available for research on gun development and photocathode activation independent of beamtime at the S-DALINAC [11, 12]. It features a chamber for photocathode activation as well as a 60 kV DC photo-gun with adjacent diagnostics beamline. Recent research at Photo-CATCH has focused on enhancing the surface layer and optimizing the activation process [12, 13].

2. Activation of GaAs photocathodes

The photoelectric threshold of GaAs, i.e. the sum of the band gap energy E_g and the electron affinity E_A, is about 5.5 eV [14], corresponding to an incident wavelength of 225 nm. However, in order to attain electron emission with high spin-polarization, excitation at photon energies in the range of $E_g < E_\gamma < E_g + \Delta_{so}$ is required, with the spin-orbit split-off energy Δ_{so} of GaAs [15]. This corresponds to a range of 1.42 eV to 1.70 eV or 730 nm to 870 nm. The main limiting factor is the electron affinity of the clean semiconductor surface, about 4.1 eV for GaAs. It can be effectively reduced to zero and even to negative values by applying a thin surface layer of Cs and further adding O (or another oxidant such as NF_3) to the Cs-layer, creating an NEA photocathode [14].
This surface layer is added during the actviation process, requiring the photocathode to be placed in an ultra-high vacuum (UHV) environment with a base pressure below 10^{-10} mbar and the prior

removal of any contaminants on the surface. Cs and O are then added in a particular order and amount, called activation scheme, to form the surface layer. While O is typically introduced in the form of O_2 gas through a leak valve, Cs is commonly provided by a vapor dispenser. In this work, the so-called co-deposition (Co-De) scheme as described in [16] was used. Cs is added first at an optimized rate until the photocurrent reaches a saturation maximum, the so-called Cs peak, after which the photocurrent begins to decline due to oversaturation of the surface with Cs. Either at the Cs peak or after a short decline of photocurrent, O is introduced at a set level of exposure. The photocurrent then rises again until a saturation plateau is reached, at which point both Cs and O exposure is halted.

Two conditional factors are crucial for the outcome of the Co-De scheme: the rate of Cs exposure, and the ratio of Cs to O exposure. The former influences the overall length of the activation process, as well as the resulting photocathode lifetime: if too little Cs is added, the NEA layer will not form fast enough to prevent residual gas adsorption from disturbing the structure of the layer. If too much Cs is added, the layer will not be thin enough to allow undisturbed electron emission, hence reducing η. The impact of the Cs rate is also directly connected to the ratio of the two ingredients: an optimal balance of Cs and O must be kept in order to create an NEA layer with ideal structure. If too little O is added, the activation will be incomplete since further addition of O would continue increasing η. Too much O impedes the rise of photocurrent, effectively ending the activation process prematurely at a greatly reduced final η. Hence, the rate of O exposure must be adjusted to the rate of introduced Cs at an optimal ratio.

3. Automated activation at Photo-CATCH

3.1 Setup

The measurements described in this work where conducted in the activation chamber of the Photo-CATCH setup. A base pressure as low as 1×10^{-11} mbar after bakeout is provied by one IG pump and one NEG pump and measured using a cold-cathode ionization gauge[1] connected to a remote-controllable multi-channel gauge controller[2]. The molybdenum photocathode holder is placed on a carousel assembly that allows both vertical and radial movement. For heat cleaning of the surface, two heating coils are available. For activation, the photocathode is placed above a ring anode and a Cs vapor dispenser. For the measurements presented here, the ring anode was connected to a powersupply to provide a bias voltage of 102 V, and to an ADC to measure the photocurrent. Oxygen is introduced from an external reservoir through a piezoelectric leak-valve that is controlled by a precision high-voltage module[3]. A laser diode[4] was mounted on an adjacent laser table and provided incident light with $\lambda = (780 \pm 5)$ nm and P_L in the low μW range through a fiber optic patch cable. The components are connected to an EPICS IOC server for remote control and data acquisition. A dedicated GUI created with Control System Studio is used to perform and monitor the activation process.

[1] Pfeiffer Vacuum®IKR 270 compact cold cathode gauge
[2] Pfeiffer Vacuum®TPG 366 Maxigauge
[3] Iseg®DPSmini DPp 10 805 24 5 M_SHV
[4] Roithner Lasertechnik RLT780-150GS

3.2 Procedure

Since the Co-De procedure requires the least steps during activation, it was chosen as basis to devise a simple, proof-of-principle automated activation scheme. For this purpose, the Co-De procedure is characterized by two time intervals: the total duration of the activation, equivalent to the duration t_{cs} the Cs dispenser is switched on, and the duration of oxygen exposure t_{ox}. Both durations depend on the respective exposure rates. At Photo-CATCH, the rate of exposure is determined by the partial pressures p_{cs} and p_{ox} of Cs and O_2, respectively. The value of p_{cs} is defined as the difference between the pressure p_1 at the beginning of the Cs peak and the initial pressure at the beginning of the activation procedure p_0. Similarly, p_{ox} is then defined as the difference between the pressure during oxygen exposure p_2 and p_1. The ratio of Cs to O exposure is then given as $r = p_{cs}/p_{ox}$. For the Photo-CATCH activation setup, an optimal ratio of $r_{opt} = 0.043$ was established during previous studies [17]. The flux rates of Cs and O are adjusted by the vapor dispenser operating current I_{cs} and the piezo-electric leak valve operating voltage U_{ox}. For manual activations, it is common to choose a setpoint for both parameters and then adjust them during the procedure to maintain the desired partial pressure. Since the partial pressures had to be maintained manually at the time of the measurements presented in this work, the setpoints of I_{cs} and U_{ox} were used for the automated scheme.

Hence, a basic automated scheme can be carried out by using timers to switch Cs and O exposure on and off at given operating value setpoints. The values of the four parameters of this automated scheme were extracted from previous manual activations: $t_{cs} = 39\,\text{min}$, $t_{ox} = 22.8\,\text{min}$, $I_{cs} = 3.1\,\text{A}$, corresponding to $p_{cs} = (5.5 \pm 0.5) \times 10^{-11}\,\text{mbar}$, and $U_{ox} = 580\,\text{V}$, corresponding to $p_{ox} = (1.3 \pm 0.1) \times 10^{-9}\,\text{mbar}$. A total of 9 activations were carried out using this automated scheme at $P_L = (8 \pm 2)\,\mu\text{W}$. Additionally, a total of 5 manual activations at $P_L = (5 \pm 1)\,\mu\text{W}$ were conducted for comparison. The photocathode was heat-cleaned in the activation chamber before each activation at a temperature of about 500 °C.

3.3 Results and Discussion

The final values of η for both automated and manual activation series are shown in fig. 1. Automated activation No. 9 only reached a final η of (0.2 ± 0.1) % due to excessive oxygen exposure, causing a premature saturation of the photocurrent. It was therefore deemed a failed activation and omitted from fig. 1. The observed fluctuations in η between the individual activations are within the range usually observed at this activation setup. In total, the successful automated activations yielded a lower mean final quantum efficiency $\overline{\eta}_{auto} = (4.9 \pm 0.8)$ % compared to $\overline{\eta}_{man} = (6.0 \pm 0.6)$ % of the manual activations, corresponding to a factor of 0.8 ± 0.2. Nevertheless, the automated scheme showed a good reproducibility at a moderate failure rate of 1 out of 9.

For further analysis, the photocurrent trend of each automated activation was scrutinized and compared with the nominal trend for a Co-De activation. Only 3 out of 9 activations showed the expected trend. 5 out of 9 activations appeared to be stopped prematurely, before a saturation plateau in photocurrent was reached during oxygen exposure. Taking the failed activation No. 9 into account, three different trends can be attributed to the level of oxygen exposure: 1) If an adequate level is introduced, the photocurrent trend is as expected. 2) If a lower level is introduced, the activation ends prematurely at a lower η since more oxygen would be required to reach photocurrent

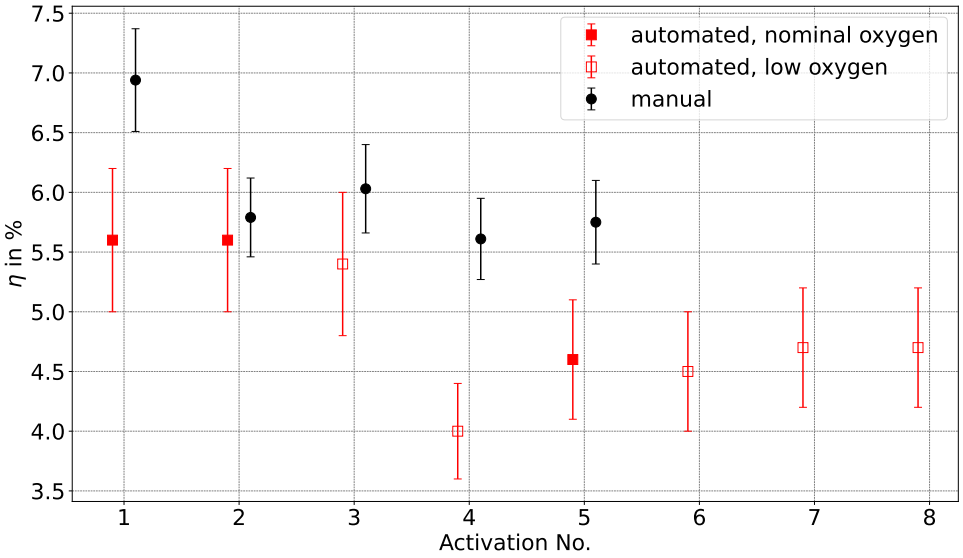

Figure 1: Final quantum efficiencies for both automated and manual activations, in chronological order. Automated activation No. 9 was deemed a failure and is not shown.

saturation. 3) If a higher level is introduced, saturation occurs too early and the resulting η is lower. A comparison of the different photocurrent trends is shown in fig. 2. The automated activations of the cases 1) and 2) yielded $\overline{\eta}_{\text{auto},1} = (5.3 \pm 0.6)\,\%$ and $\overline{\eta}_{\text{auto},2} = (4.7 \pm 0.5)\,\%$, respectively. Hence, for the intended exposure levels, the automated procedure yielded results well comparable to the manual procedure, corresponding to a factor of 0.9 ± 0.2 compared to manual activation. An overview of the mean final quantum efficiencies is shown in tab. 1.

Table 1: Resulting mean final quantum efficiencies for the manual and automated Co-De activation schemes.

Scheme	case	# of activations	$\overline{\eta}$ in %
manual	total	5 of 5	6.0 ± 0.6
automated	total	9 of 9	4.4 ± 1.6
	successful	8 of 9	4.9 ± 0.8
	nominal oxygen	3 of 9	5.3 ± 0.6
	low oxygen	5 of 9	4.7 ± 0.5
	high oxygen	1 of 9	0.2 ± 0.1

The fluctuation in oxygen exposure was traced back to the behaviour of the pieco-electric leak valve, as a variation of p_{ox} was observed for the given U_{ox} setpoint. Also, the oxygen flux does not remain constant for a given setpoint, but increases over time. During manual activations, this is rectified by manually adjusting U_{ox} such that the overall chamber pressure, and therefore r, remains constant. Hence, an automated oxygen exposure level control is required to improve the reproducibility of the automated scheme. Also, a long-term change of p_{cs} between activations could be observed for the

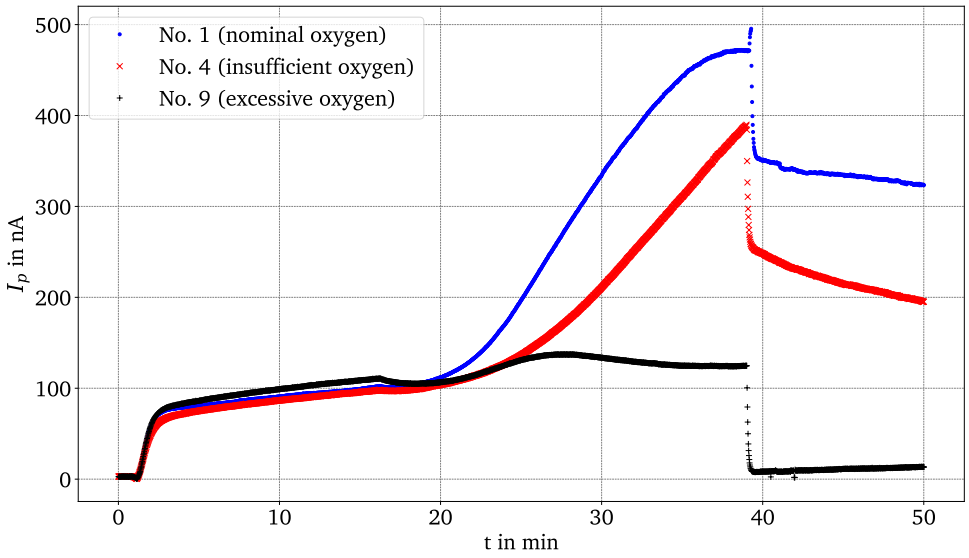

Figure 2: Photocurrent trends over time of automated activations No. 1 (top curve), No. 4 (middle curve) and No.9 (bottom curve), corresponding to nominal oxygen exposure, insufficient oxygen exposure, and excessive oxygen exposure, respectively.

given I_{cs} setpoint, as well as a slow increase during activation due to heating of the vapor dispenser during operation. This can be addressed by implementing an online calculation of p_{cs}, allowing automated online adjustment of the Cs exposure rate.
It is also important to note that the manual and automated series were conducted with two different photocathode samples. After the automated series was conducted, the activation chamber had to be vented and opened for mechanical repairs. The photocathode was subsequently replaced with a new sample, freshly cut from a GaAs wafer, for the manual series. Hence, the lower quantum efficiencies observed during the automated activations may in part be attributed to the wear of the used sample from previous activations.

4. Conclusion and Outlook

A first successful proof-of-principle test of a basic automated activation procedure has been conducted, yielding no significant decrease in final quantum efficiencies compared to manual activation within the uncertainties for nominal levels of oxygen exposure. Even for lower levels of oxygen exposure, reasonable final quantum efficiencies were obtained, with only 1 out of 9 automated activations failing due to oxygen overexposure. The devised scheme is a promising basis for further development of automated activation procedures. Implementation of automated online exposure rate adjustment for both Cs and O is expected to greatly increase the performance of the automated process, allowing for optimized activation procedures without expert operator input. Further development of the automated activation procedure as well as studies on the resulting photocathode quantum efficiency and lifetime are planned at Photo-CATCH.

References

[1] C.K. Sinclair, *DC photoemission electron guns as ERL sources*, *Nuclear Instruments and Methods in Physics Research Section A: Accelerators, Spectrometers, Detectors and Associated Equipment* **557** (2006) .

[2] T. Rao et al., *Photocathodes for the energy recovery linacs*, *Nuclear Instruments and Methods in Physics Research Section A: Accelerators, Spectrometers, Detectors and Associated Equipment* **557** (2006) .

[3] D. Abbott, P. Adderley, A. Adeyemi, P. Aguilera, M. Ali, H. Areti et al., *Production of highly polarized positrons using polarized electrons at MeV energies*, *Phys. Rev. Lett.* **116** (2016) 214801.

[4] L.S. Cardman, *The PEPPo method for polarized positrons and PEPPo II*, *AIP Conference Proceedings* **1970** (2018) 050001.

[5] A. Brachmann, J.E. Clendenin, E.L. Garwin, K. Ioakeimidi, R.E. Kirby, T. Maruyama et al., *The polarized electron source for the international collider (ILC) project*, *AIP Conference Proceedings* **915** (2007) 1091.

[6] G. Moortgat-Pick, T. Abe, G. Alexander, B. Ananthanarayan, A. Babich, V. Bharadwaj et al., *Polarized positrons and electrons at the linear collider*, *Physics Reports* **460** (2008) 131.

[7] J. Skaritka, E. Wang, F. Willeke, R. Lambiase, W. Lui, V. Ptitsyn et al., *Conceptual design of a Polarized Electron Ion Collider at Brookhaven National Laboratory*, *Proceedings of XVII International Workshop on Polarized Sources, Targets and Polarimetry — PoS(PSTP2017)* **324** (2018) 015.

[8] N. Pietralla, *The Institute of Nuclear Physics at the TU Darmstadt*, *Nuclear Physics News* **28(2)** (2018) 4.

[9] M. Arnold, J. Birkhan, J. Pforr, N. Pietralla, F. Schließmann, M. Steinhorst et al., *First operation of the superconducting Darmstadt linear electron accelerator as an energy recovery linac*, *Phys. Rev. Accel. Beams* **23** (2020) 020101.

[10] Y. Poltoratska, C. Eckardt, W. Ackermann, K. Aulenbacher, T. Bahlo, R. Barday et al., *Status and recent developments at the polarized-electron injector of the superconducting Darmstadt electron linear accelerator S-DALINAC*, *Journal of Physics: Conference Series* **298** (2011) 012002.

[11] M. Herbert, J. Enders, Y. Fritzsche, N. Kurichiyanil and V. Wende, *Inverted Geometry Photo-Electron Gun Research and Development at TU Darmstadt*, *Proc. 9th International Particle Accelerator Conference (IPAC'18), Vancouver, BC, Canada, April 29-May 4, 2018* (2018) 4545.

[12] N. Kurichiyanil, J. Enders, Y. Fritzsche and M. Wagner, *A test system for optimizing quantum efficiency and dark lifetime of GaAs photocathodes*, *Journal of Instrumentation* **14** (2019) P08025.

[13] M. Herbert, *Electron emission from GaAs photocathodes using conventional and Li-enhanced activation procedures*, doctoral dissertation, Technische Universität, Darmstadt, 2022. doi:10.26083/tuprints-00020707, http://tuprints.ulb.tu-darmstadt.de/20707/.

[14] W.E. Spicer and R.L. Bell, *The III-V photocathode: A major detector development*, *Publications of the Astronomical Society of the Pacific* **84** (1972) 110.

[15] D.T. Pierce and F. Meier, *Photoemission of spin-polarized electrons from GaAs*, *Phys. Rev. B* **13** (1976) 5484.

[16] H. Sonnenberg, *Long-wavelength photoemission from InAs1-xPx*, *Applied Physics Letters* **19** (1971) 431.

[17] N. Kurichiyanil, *Design and construction of a test stand for photocathode research and experiments*, doctoral dissertation, Technische Universität Darmstadt, Darmstadt, Juli, 2017. http://tuprints.ulb.tu-darmstadt.de/5903/.